



Published in final edited form as:

*Lab Chip*. 2017 September 26; 17(19): 3221–3233. doi:10.1039/c7lc00623c.

## Microfluidic modeling of biophysical microenvironment in tumor cell invasion

Yu Ling Huang<sup>a</sup>, Jeffrey E. Segall<sup>b</sup>, and Mingming Wu<sup>a</sup>

<sup>a</sup>Department of Biological and Environmental Engineering, 306 Riley-Robb Hall, Cornell University, Ithaca, NY 14853

<sup>b</sup>Anatomy and Structural Biology, Albert Einstein College of Medicine, 1300 Morris Park Avenue, Bronx, New York 10461

### Abstract

Tumor cell invasion, whether penetrating through extracellular matrix (ECM) or crossing a vascular endothelium, is a critical step in the cancer metastatic cascade. Along the way from primary tumor to a distant metastatic site, tumor cells interact actively with the microenvironment either via biomechanical (e. g. ECM stiffness) or biochemical (e.g. secreted cytokines) signals. Increasingly, it is recognized that the tumor microenvironment (TME) is a critical player in tumor cell invasion. A main challenge for the mechanistic understanding of tumor cell–TME interactions comes from the complexity of the TME, which consists of extracellular matrices, fluid flows, cytokine gradients and other cell types. It is difficult to control TME parameters in conventional *in vitro* experimental designs such as Boyden Chambers, or *in vivo* such as in mouse models. Microfluidics has emerged as an enabling tool for exploring TME parameter space because of its ease in recreating the complex and physiologically realistic three dimensional TME with well-defined spatial and temporal control. In this Perspective, we will discuss designing principles for modeling the biophysical microenvironment (biological flows and ECM) for tumor cells using microfluidic devices, and the potential microfluidic technology holds in recreating physiologically realistic tumor microenvironment. The focus will be on applications of microfluidic models in tumor cell invasion.

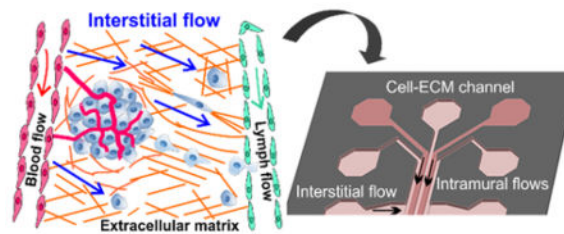
### Graphical Abstract

Microfluidic model for the physical tumor microenvironment: intramural and interstitial flows, and the extracellular matrices (ECMs).

---

#### Conflict of interest

There are no conflicts to declare.



## Introduction

Cancer metastasis of solid tumors is a physical process where tumor cells generate sufficient forces to break away from the primary tumor, invade through the interstitial extracellular matrix (ECM), squeeze through vascular vessels, and establish a secondary tumor at a distant organ<sup>1–3</sup> (Figure 1). It is now well accepted that the tumor microenvironment (TME) plays an important role, similar to the genetic makeup of the tumor cells, in determining tumor cell invasiveness. While tumor genetics has always been the focus of tumor biology, it is only in recent decades that the critical roles of the TME have been recognized widely in the context of tumor cell invasion<sup>4–9</sup>.

Broadly speaking, the complex TME can be classified into biochemical (e.g. cytokines secreted by cells and nutrients) and biophysical cues (e.g. fluid flows and ECM), as illustrated in Figure 1. Current tools for recreating the TME for tumor cell invasion are primarily Boyden chambers<sup>10–12</sup> and animal models<sup>13–15</sup>. Boyden chambers are straightforward to use, but difficult to recreate the complex TME and only provide population level and endpoint results. Animal models, on the other hand, provide a physiologically realistic environment, but are low throughput and it is difficult to isolate individual TME components. Microfluidic models have emerged to fill this gap<sup>16–21</sup>. Microfluidic models can allow for well-defined spatial and temporal arrangements of individual components of the TME, and facilitate quantitative analysis and mathematical modeling. In addition, they are compatible with optical imaging, enabling studies of single and collective cell dynamics in real time. We note that dynamic analysis is important for tumor cell invasion studies because heterogeneity and plasticity are hallmarks of cancer<sup>22–24</sup>. In this Perspective, we will focus on recent progress as well as future direction in the development of microfluidic devices for studying the roles of biophysical cues, specifically, biological flows and ECM, in driving tumor cell invasion. For microfluidic developments in the analysis of biochemical cues with applications in tumor cell invasion, please refer to recent excellent review articles<sup>16, 25–27</sup>.

## Biophysical drivers in tumor cell invasion

### Intramural flow in tumor cell invasion

Biological flows are ubiquitous in living systems and generally can be classified into intramural flows (blood and lymph flow) and interstitial flows (see Figure 1 and Table 1). Blood flow follows the large scale anatomical pattern, mainly aorta and arteries, with high flow speed in the order of tens of centimeters per second<sup>28</sup>, and branches out to smaller

scale arterioles and capillaries with lower speed, ranging from a few centimeters to a few hundred micrometers per second<sup>29</sup>. In addition to nutrients and oxygen transport, shear stress from blood flow is known to be a critical regulator in vascular physiology<sup>30</sup> and morphogenesis during development<sup>31–33</sup>, and is tightly linked to endothelial cell function<sup>34–37</sup>. Lymph flow, on the other hand, is several orders of magnitude smaller than blood flow, and has been reported to be on the order of a few millimeters per second in lymphatic vessels<sup>38</sup> and tens of micrometers per second in lymphatic capillaries<sup>39</sup>.

Blood/lymph flow within the TME is aberrant and their roles in tumor cell invasion are largely unknown (see Table 1). Similar to normal tissue, blood flow in the TME is essential for tumor perfusion and growth. Different from the flow in normal tissue, blood flow in the TME is difficult to predict because of its dynamic nature. Blood flow rates within the TME are known to change with the abnormal growth of vascular vessels through angiogenesis, the physical stress from the fast growing tumor mass, and altered ECM mechanical properties. In addition, the blood vessels within the tumor are torturous, and often lack functional pericytes, basement membrane, and tight endothelial cell junctions<sup>40–42</sup>. Lymph flow within the TME has received much less attention, but is found to be elevated in contrast to healthy tissue<sup>43</sup>.

The roles of blood/lymph flow in tumor cell invasion are often attributed to the shear force regulation at the interface with endothelial cell (EC) layers. In order to disseminate to a distant organ, tumor cells must use the blood or lymphatic vessels as a conduit, and thus need to cross the EC layer<sup>44–46</sup>. Tumor cells are unlikely to enter/leave via the aortic or arterial vessels as those vessels have thicker walls and high shear stress. In contrast, blood capillaries with thinner walls and lower shear stress are more likely to physically trap circulating tumor cells for subsequent extravasation<sup>3, 44, 47</sup>. In parallel, lymphatic capillaries with significant slower flow at the host tissue are also sites where tumor cells prefer to reside<sup>48</sup>. Taken together, flow shear stress critically regulates the physiology of the vascular EC layers, and impacts on tumor cell invasion.

### **Interstitial flow in tumor cell invasion**

Interstitial flow is a slow fluid movement through the interstitial space driven by hydrostatic and osmotic pressure differences between the arterial and venous or arterial and lymphatic vessels<sup>49, 50</sup>. First measured by the Jain lab using the fluorescence recovery after photo bleaching (FRAP) technique, the flow speed associated with interstitial flow is typically on the order of a few micrometers per second in normal tissue<sup>50</sup>. While the main function of interstitial flow has long been known to drain waste fluids to the lymphatic system, recently it has been shown to regulate vascular morphogenesis<sup>51–53</sup>.

Interstitial flow within the TME is elevated due to the heightened interstitial fluid pressure<sup>54, 55</sup> (Table 1). High interstitial fluid pressure in the TME, in part, is a result of the fact that excessive interstitial fluids could not be absorbed by the compressed non-functional lymphatic vessels within the tumor. It has been reported that the pressure is particularly high within a malignant tumor, and drops steeply at the tumor-host tissue interface<sup>55, 56</sup>. For nearly three decades, high interstitial fluid pressure has been an important biomarker for

tumor progression and a significant obstacle for cancer therapeutic delivery into the tumor 57–60.

Recently, the physical consequence of elevated and excessive interstitial fluid flow outward from the tumor to the host tissue has been investigated in the context of tumor cell invasion using *in vitro* models<sup>61–63</sup>. Using a modified Boyden chamber, the Swartz lab discovered that interstitial flow can guide tumor cell invasion along the flow direction. The unique feature of interstitial flow is that it operates in a region where the Peclet number (convective versus diffusive transport) is close to one. In other words, the transport of secreted cytokines is governed by both convective flow and diffusion. Computation of cell secreted cytokine transport shows that interstitial flow leads to flow-induced spatial gradients of secreted cytokines<sup>52</sup>. One example is the spatial gradients of lymphatic chemokine CCL19/21 along the flow direction, and breast tumor cells were discovered to follow the flow/gradient direction using a modified Boyden Chamber model<sup>61</sup>. More recently, interstitial flow was found to directly impact tumor cell mechanotransduction via CD44 in brain tumor cells<sup>64</sup> and via integrins in breast tumor cells<sup>65</sup>. Interstitial flow also has been shown to promote tumor cell invasion via stromal cell mediated matrix remodeling within the TME<sup>66</sup>. In summary, mounting evidence demonstrates that interstitial flow critically modulates tumor cell invasion behavior.

### Extracellular matrix in tumor cell invasion

The extracellular matrix (ECM) is a major physical component that surrounds and penetrates solid tumors. Important physical ECM characteristics that are critical for tumor cell invasion include ECM overall stiffness and architecture<sup>67, 68</sup>. Stiffness, contributed mainly by dense and cross linked ECM fibrillar structures, is a prognostic and risk factor for breast cancer patients<sup>69, 70</sup>. Similarly, increasing evidence demonstrates that stiffer ECM promotes tumor cell invasion in *in vitro* assays<sup>5, 71</sup>. It has been found that malignant tumor cells and tumor associated stromal cells secrete collagen, which contributes to dense fibrillar structures<sup>71</sup>. They also express enzymatic cross linkers, such as lysyl oxidase, which increase the overall stiffness of the ECM<sup>72, 73</sup>. Breast tumor has been reported to be twenty times stiffer than the normal breast tissue<sup>5</sup>.

Recent developments in intravital imaging reveal that tumor ECM is highly heterogeneous in space, and evolves with time<sup>74–76</sup>. This is not surprising because tumor and stromal cells are known to actively pull onto the ECM, and thereby remodel the ECM architecture<sup>66, 77, 78</sup>. Collagen bundles have been reported to align perpendicularly to the tumor periphery, possibly by active tumor and stromal cell contraction, facilitate collective tumor cell invasion and correlate with malignancy<sup>79, 80</sup>. Micro-tunnels, hollow micro-sized tunnels with diameter range of 1–30  $\mu\text{m}$ , were recently observed to provide tumor cells fast moving pathways both *in vitro* and *in vivo*<sup>81–83</sup>. These hollow micro-sized tunnels are created by the degradation of collagen matrices via matrix metalloproteinase (MMP) secreted by the tumor and stromal cells. In the context of ECM architecture, the three dimensional nature of the ECM has been discussed extensively in the cell migration community and can be a critical regulator of cell migration<sup>84–86</sup>.

## Microfluidic modeling of the biophysical parameters in the tumor microenvironment

Microfluidics has emerged to model the TME because of its tight control of flow rates within a 3D ECM. A good microfluidic model needs to be able to recreate blood/lymphatic vessels of appropriate physiological size and shape within a 3D ECM, with controlled flow rates. In addition, the microfluidics should be robust and high throughput. Here, we discuss current efforts in modeling the biophysical aspects of the TME using microfluidic devices. The goal is to create on chip vascular vessels and ECM with architecture, dimensions and flow rates closely mimicking the in vivo measurement results (see Table 1). We emphasize the mathematical modeling of the flow rates/shear stress within the microfluidic platform using the relevant physical parameters including vascular permeability of endothelium layers and hydraulic conductivity of ECM (see Table 2).

### Microfluidic models for intramural flow in tumor cell invasion

A critical step for modeling intramural flow in the context of tumor cell invasion is to engineer a perfusable and functional vascular tube/network within a 3D ECM. Motivated by the development of vascularized biomaterial, early work began with the engineering of an EC tube in one single microfluidic channel within dense type I collagen matrices. The microfluidic channel was created through a micro-molding method, in which a hypodermic needle or a microfabricated PDMS positive channel feature was used as a template, and hydrogels as molding materials. After removing the template, endothelial cells were introduced into the channel and formed an EC monolayer<sup>87–92</sup>. A recent alternative method for creating a single EC tube is through introducing a less dense fluid into a dense fluid (un-polymerized collagen) via a process known as viscous fingering<sup>93–95</sup>. This method does not require microfabrication thus is cost effective, the downside being that it lacks precise control over the size of the vessel.

More complex 3D vascular networks embedded within synthetic or naturally derived matrices have been developed recently using a sacrificial method<sup>96–100</sup>. Here, one first creates an interconnecting fiber network using either microfabrication or 3D printing with sacrificial materials that are compatible with cell culture (e.g. gelatin and carbohydrate glass). The polymerized gelatin or solidified carbohydrate glass fiber network is then submerged within synthetic or naturally derived gels. After removing the sacrificial layers, ECs are introduced into the network to form lumens. We note that autonomous formation of microfluidic vascular networks by placing ECs in biomatrices along with a set of well-defined reagents and/or fluid flow that promote angiogenesis<sup>101–103</sup> and lymphangiogenesis<sup>104</sup> have been successful and been used in the context of drug delivery. This method can potentially be introduced for the purpose of tumor cell invasion.

An important way that intramural flow regulates tumor cell intravasation/extravasation is through the alteration of EC layer integrity and permeability via flow induced shear stress (See Table 2). A key parameter that is commonly used to characterize the transport of solute across an endothelium layer is the permeability coefficient,  $P(\text{cm/s})$ , which is defined as  $J_s/\nabla C$ , where  $J_s(\text{g/cm}^2/\text{s})$  is the solute flux through an unit area,  $\nabla C(\text{g/cm}^3)$  is the spatial

gradient of solute concentration. In Table 2, we list permeability of both blood and lymphatic vessels measured in healthy and tumor tissues. It is interesting to note that one *in vivo* study by Gerlowski *et al.* revealed that the vascular permeability is significantly increased in tumor compared to normal vasculature<sup>105</sup>, echoing the notion that tumor vasculature is leakier than healthy vasculature. We also note that error bars for these measurements are typically large. Looking forward, the microfluidic platform allows us to make precise spatial arrangement of solute concentration, obtain temporal information of the concentration field, and thus has the potential to improve the permeability measurements in the future.

Shear stress from the intramural flows are known to alter EC permeability as well as integrity. Flow induced shear stress has been reported to increase the barrier function or lower the permeability coefficient of the EC layer<sup>92, 106, 107</sup> and suppress VEGF-driven EC sprouting<sup>108</sup>. Progress has been made to incorporate tumor cell laden ECM into a single engineered microfluidic blood vessel or vascular networks for dynamic tumor trans-endothelial migration<sup>89, 92, 107, 109–111</sup>, making it possible to examine quantitatively the impact of intramural flow on tumor cell invasion. Using a microfluidic model, we have learned that blood flow through the capillaries reduces tumor cell extravasation rates<sup>107</sup>. This is not surprising because the EC layer junction is strengthened under flow shear stress, and increases its ability to prevent transmigration. It is interesting to note that lymph flow on the other hand, promotes intravasation using a flow chamber modified from the Boyden chamber<sup>112</sup>. This discrepancy can likely be explained by the differential responses of blood and lymphatic vessels to flow shear stress. In this context, a tight control over the flow rates, in which microfluidic models have the advantages over other conventional models, will allow us to gain a deeper understanding of the impact of intramural flow on tumor cell transmigration.

### Microfluidic models for interstitial flow in tumor cell invasion

Broadly speaking, there are two types of assays for creating interstitial flows. One is the modified Boyden Chamber assay and the other is the microfluidic platform (See Fig. 2). The modified Boyden Chamber assay uses a commercially available platform, and is straightforward to implement, but results are population based and end points. The microfluidic platform, on the other hand, allows for dynamic and single cell imaging, but is typically difficult to make, requiring engineering training for the users. Here, we discuss the evolution of several platforms developed to date for creating interstitial flows. We will highlight biological insights gained using these platforms in the context of tumor cell invasion.

Pioneering work on roles of interstitial flows in tumor cell invasion was carried out in a modified Boyden chamber<sup>61</sup>. A layer of tumor cell embedded biomatrix was introduced into the insert of a Boyden chamber. Interstitial flow is gravity driven, facilitated by the fluid level difference between the fluid within the insert and the cup surrounding it (Fig. 2A). Type I collagen, a main structural component of mammalian tissue, has been used in most of the current studies for its ability to mimic *in vivo* ECM architecture and compatibility with cell invasion assay<sup>83</sup>. In addition, the mechanical properties<sup>78, 113, 114</sup> and specific



hydraulic conductivities (see Table 2) of collagen gels have been studied and documented extensively in the literature from the biomaterials community. Here, the readout is the number of cells transmigrated through the porous membrane. Using the modified Boyden chamber, a number of biological insights have been gained<sup>61, 63</sup>, most notably the autologous chemotaxis of breast tumor cells mediated by flow induced lymphoid chemokine gradients.

Although the modified Boyden chamber assay is straightforward to use, the results are population based and end points. One of the hallmarks of tumor cells is the heterogeneity of a single cell population. It is thus important to develop assays that are amenable to single cell analysis. Microfluidic platforms have emerged to model interstitial flows. A critical component for modeling interstitial flow through 3D ECM in a microfluidic platform is to confine natively derived or synthetic ECM within an area where fluid flow can be applied through the ECM in a controlled way. To create a microfluidic platform for tumor cell invasion in the presence of interstitial flow, a number of labs have developed unique microfabrication methods to pattern type I collagen in a three parallel channel configuration<sup>65, 115–118</sup>. The common feature of all the devices is to develop micro-patterned structures to confine biomatrices in designated places. In the work of Hassler *et al.* or Polacheck *et al.*, tumor cells embedded in collagen (unpolymerized) are introduced into a channel lined with two parallel lines of micropillars (see red or green channel in Figure 2. B and C). Interstitial flow is introduced in the horizontal direction after gel polymerization. This configuration has advantages over the early engineering method for vascular tube using micro-molding method for its flexibility of the channel layout, and also for its ease of integrating tumor cells within ECM. The use of spaced micropillars utilizes surface tension to confine the unpolymerized collagen solution, while leaving space between the micropillars for interstitial flow to pass through the polymerized collagen matrices. This method offers robust confinement of the ECM, but the micropillars block a significant amount of the flow and complicate the spatial distribution of the flow field (see right panel in Figure 2. B). To overcome this limitation, our lab confined cell-embedded collagen using a contact line pinning method<sup>117, 118</sup>. In our work, parallel PDMS microridges (or contact lines) with a cross section of 10  $\mu\text{m}$  by 5  $\mu\text{m}$  were fabricated to confine collagen within a wall-less channel. This method allows interstitial flow to run through the collagen matrices with over 80% spatial uniformity in the area of interest. For details of the device designs, see Figure 2D.

Darcy's law is often useful for computing interstitial flows during the device design stage. For a given layout of the device, one can compute accurately the flow rates in different parts of the channels by applying the Brinkman equation in a multi-physics software package such as COMSOL. A key parameter required is the hydraulic conductivity,  $K'$ , of the biomatrices. Hydraulic conductivity is defined through Darcy's law,  $K' = J/\nabla P$ , where  $J$  is the fluid flux,  $\nabla P$  is the spatial pressure gradient. Because of the small dimension of the system, fluid flows are slow, and Darcy's law is typically valid<sup>117</sup>. Values of hydraulic conductivity of healthy and tumor tissue, as well as reconstituted ECM are listed in Table 2. We note that hydraulic conductivity times fluid viscosity,  $K' \eta$ , named specific hydraulic conductivity ( $K$ ), is typically reported in *in vitro* ECM measurements.

Using the microfluidic platform developed, we have started to learn how interstitial flows modulate tumor cell heterogeneity and plasticity. This information is difficult to obtain in population level assays such as the Boyden Chamber assay. Haessler *et al.* showed that interstitial flow at flow speed of 10  $\mu\text{m/s}$  enhanced a subpopulation of breast tumor cell migration, highlighting the heterogeneous nature of tumor cells within a single population <sup>116</sup>. Work in our lab demonstrated that interstitial flow at flow speed of 2  $\mu\text{m/s}$  promotes amoeboid over mesenchymal motility of breast cancer cell invasion by carrying away adhesion molecules such as fibronectin. Cells lacking adhesion contacts prefer to migrate via amoeboid motility <sup>118</sup>. These studies revealed critical information on how interstitial flow influences tumor cell invasion at the single cell level and the dynamic interaction of tumor cells with their environment. The Kamm lab learned that interstitial flow can impact tumor cell migration directly via chemosensing or mechanosensing molecules. In the case of chemosensing, Polacheck *et al.* demonstrated that interstitial flow at flow speeds of 0.3 and 3.0  $\mu\text{m/s}$  induced directional migration of breast tumor cells along/against the flow direction in a chemokine receptor CCR7 dependent manner <sup>115</sup>. In later work from the Kamm lab, they reported that the directional migration of breast tumor cells along/against interstitial flow was triggered by mechanosensing molecules <sup>65</sup>.

Taken together, quantitative understanding how interstitial flow impacts tumor cell invasion within 3D ECM has just begun. Results from these studies are far from converging into a coherent theoretical understanding. Current reported results are very sensitive to experimental conditions, and differ from lab to lab. In particular, it is known that the conditions under which collagen is polymerized is critical in determining collagen fiber architecture, including PH <sup>119</sup>, polymerization temperature <sup>120</sup>, as well as the actual reagents used. It is thus of paramount importance to carefully record all the detailed cell culture condition for an eventual unified understanding. Looking ahead, many questions remain to be explored. The comparative roles of chemosensing or mechanosensing in the presence of interstitial flow remain to be investigated, as well as whether interstitial flow drives collective cell migration <sup>121</sup>. The latter is important because increasing evidence has suggested that collective cell migration may contribute to cancer cell survival and successful metastasis <sup>122–124</sup>. Current studies are limited to mainly breast tumor cells, but similar microfluidic platforms can be easily extended to study other cell types such as brain tumor cells <sup>63, 64</sup> and ovarian tumor cells <sup>125</sup>.

### **Microfluidic models for coupling intramural and interstitial flows in tumor cell invasion**

*In vivo*, both interstitial flow and intramural flow coexist. Recent progress has been made in recreating both interstitial and intramural flows within one experimental setup in the context of tumor cell invasion. Tung *et al.* developed a microfluidic device that allows for the introduction of intramural flow, and at the same time controlling interstitial flow. This device can potentially be used to study tumor cell invasion and transmigration in the presence of both flow types <sup>117</sup>. The Swartz lab developed an experimental platform that integrates a Boyden chamber and a flow channel, in which interstitial flow was introduced through the Boyden chamber and intramural flow was introduced through a flow channel underneath the Boyden chamber <sup>112</sup>. Using this platform, they revealed for the first time that interstitial flow and lymph flow synergistically increase tumor cell transmigration rates through lymphatic



vessels. We note that currently, microfluidic platforms that include both interstitial and intramural flows for tumor cell transmigration are at early stages of development.

### Microfluidics for modeling ECM architecture in tumor cell invasion

Microfabricated devices provide a unique opportunity for decoupling the contributions of individual ECM properties (e.g. alignment and pore size) from tumor cell invasion, enabling a mechanistic understanding of cell-ECM mechanical interactions.

Two important features within the TME that promote fast and persistent tumor cell invasion are aligned collagen fibers and embedded hollow micro-sized tunnels. To investigate molecular mechanisms that cells use to migrate along 1D collagen fibers, synthetic 1D tracks have been fabricated, including nano/microfabricated topographic lines and fibronectin lines that have line widths ranging from submicrometer to tens of micrometers<sup>84, 126, 127</sup>. While these engineered lines are straightforward to produce and easy to manipulate, the disadvantage is that these lines are made on a 2D surface which do not recapitulate the 3D *in vivo* situation where cells are supported by fiber network around all surfaces. Alternative methods have been developed to circumvent this limitation. One way of producing aligned collagen fibers within a 3D ECM is to use shear stress. One can flow unpolymerized collagen through a micro-sized channel in microfluidics, and the flow shear force has been shown to be able to align collagen fibers along the flow direction<sup>128–131</sup>. A second method is to flow a less dense collagen solution (low concentration) into a dense solution (Matrigel solution at high concentration) within a channel to form aligned collagen fibers at the gel interface<sup>132</sup>. A third method is to repeatedly stretch and relax a collagen fiber network already polymerized on a 2D substrate<sup>133</sup>. Recently, self-assembled micro-sized magnetic bead strings embedded within hydrogel have been used as mimics of 3D collagen fibers for the purpose of tumor cell invasion studies<sup>134</sup>. These studies revealed that alignment promote directional cell migration by limiting the cellular protrusion sites within the line/fiber or contact guidance. In addition to 1D topography, confined micro-tunnels have been discussed extensively as a highway for tumor cell migration recently. Microfabricated tunnels/channels surrounded by collagen provide a controlled way to study molecular mechanisms that cells use to migrate through these tunnels. Interestingly, MMPs are required for making these micro-tunnels in the first place, but then existing microfabricated tunnels facilitate MMP independent tumor cell invasion<sup>135, 136</sup>.

A limiting factor for tumor cell migration within the 3D ECM network is the nucleus, which is the stiffest part of a cell. It has been reported that tumor cells fail to migrate when their nucleus size is larger than the ECM pore size<sup>137</sup>. To understand the nuclear mechanics, microfluidic models have been developed to precisely mimic the constrictions presented to the cells by the ECM pores. Here, an array of micropillars with a few micrometers spacing is fabricated on a substrate<sup>138–140</sup>. Nuclear envelope rupture and DNA damage is observed when tumor cells squeeze through gaps with spacing smaller than the nucleus. Interestingly, the majority of tumor cells are seen to self repair and survive<sup>140, 141</sup>.

With the rapid progress in biomaterials, we can now fine tune the stiffness of type I collagen as well as its architecture individually or together, enabling a mechanistic understanding of the role of mechanical properties of ECM in tumor cell invasion. Increasing collagen

concentration is a simple and straightforward method for increasing gel stiffness, however, this generates significant smaller pore sizes at the same time<sup>137, 142, 143</sup>. A number of other techniques have been developed to increase the collagen stiffness without altering the concentration, they include varying polymerization temperature<sup>120, 144</sup> and pH<sup>119</sup>, nonenzymatic cross-linking of the fibers<sup>145, 146</sup>, and applying mechanical tension<sup>129, 147</sup>. Future development requires integrating these biomaterial manipulation techniques with microfabricated device to pattern precisely the matrix stiffness or pore size in space for high throughput studies of tumor cell-ECM interactions.

## Opportunities, challenges and future perspective

The biophysical microenvironment critically regulates tumor cell invasion. To date, the majority of the cell and drug screening experiments *in vitro* are carried out in static conditions, whereas biological flows are everywhere in the human body. Incorporating flows in tumor cell invasion experiments and beyond could potentially revolutionize our understanding in cancer biology. One can foresee the incoming impact will be similar to the impact brought by using 3D ECM in comparison to 2D platform for *in vitro* tumor cell invasion studies. Looking ahead, several challenges require our immediate attentions.

## Recapitulating the complex tumor biophysical microenvironment

Microfluidic models have enabled us to learn the individual roles of ECM mechanical properties, intramural and interstitial flows in tumor cell invasion. However, synergistic roles of multiple biophysical factors remain to be explored. Microfluidic devices provide a unique opportunity here, because one can easily introduce biophysical parameters into the platform in a reconfigurable way. An example of such a device is illustrated in Fig. 3, where biophysical parameters including intramural and interstitial flows can be added or subtracted with ease. Here, two vascular vessels are created mimicking blood and lymphatic vessels respectively, with tumor cells embedded within ECM placed adjacent to the vascular vessels. In this platform, one can fine tune intramural, interstitial flows and ECM stiffness or pore sizes while observing tumor cell dynamic behavior at the same time. This capability allows for a basic understanding of how these three physical parameters synergistically influence tumor cell invasion within a complex and well-defined TME.

Biochemical environments such as cytokine gradients are traditional driving forces for tumor cell invasion, and are coupled with the biophysical environment. Towards this end, it will be important to first learn how biochemical gradients influence tumor cell invasion<sup>148</sup>, and incorporate this information into the biophysical models proposed. Microfluidic models such as the one shown in Figure 3 can be easily used to generate cytokine gradients to meet this purpose. For example, we can flow cytokine and buffer respectively into the arteriole and venule channels, and a cytokine gradient can be established within the tumor embedded ECM space. The integration of biochemical and biophysical environments will be an important step towards a physiologically realistic microfluidic model.

### Creating robust and highly reproducible platforms

Despite the aforementioned many advantages of using microfluidic models, microfluidic technology is still at an early stage, and is not widely accepted by many cancer biology labs. The bottlenecks are availability, ease of use, robustness and reproducibility. Most microfluidic models require engineering training for their use. To make a higher impact in cancer biology, it is important to design devices that are simple in concept, easy to use, and compatible with conventional biology labs. Partnering with industry is one possible route to make microfluidic models available to wider communities<sup>19</sup>. Various agencies such as National Institute of Health provide special funds (e. g. SBIR) to encourage industry/academy partnerships. It is commendable that many research groups have now taken the lead in translating their microfluidic tools into the commercial space. Recent development in 3D printing technologies enables production of assembly-free microfluidics and eliminates the need of microfabrication for devices at micrometer or millimeter length scale<sup>149</sup>. For ease of use, applying the physical principle of fluids (viscous fingering) to make an EC tube or vascular network within a channel is an alternative method to fabricating complicated features on a device<sup>93</sup>. In addition, a design with gravitational driven flow will be more favorable than using pumps to create biological flows through a channel.

### Developing quantitative analysis tools for understanding cell-environment interaction

Microfluidic devices allow us to collect large amounts of quantitative information. However, to make sense of the data, or to come up with a theoretical framework of the subject being investigated, it is important to develop quantitative analysis tools. For understanding the roles of physical parameters in tumor cell invasion, one useful tool is to track tumor cells in 3D in an automatic way. Commercial software such as Imaris has made significant progress in this direction, however, it still cannot handle the dynamic variability of tumor cells. A particularly difficult situation is when a cell dynamically changes its shape and merge and then dissociate with another cell in a trajectory - the tracking program does not have the ability to follow the cells. Recent advances in computer vision and machine learning could potentially resolve tracking of the shape and position of the moving cancer cells in space and time. A second tool is cell traction force measurements in 3D. The key regulator for cell-physical environment interaction is cell generated force. A number of 3D single cell traction force microscopy methods have been developed for measuring cell generated forces, but are far from easy to use, and are limited to a few labs around the world at the moment<sup>78, 150, 151</sup>.

### Outlook

Cancer cells are known to be heterogenous phenotypically and genetically. The altered tumor physical microenvironment, e.g. matrix spatial restriction<sup>152</sup>, is a highly relevant contributor to the phenotypic and genetic instability of the invading tumor cells. An ultimate solution to the problem is to reveal molecular and cell level information simultaneously with a controlled microenvironment at single cell level. Recent developments in biosensors (mechanosensors and chemosensors) has made this possible. In addition, microfluidics with on chip polymerase chain reaction capability can be incorporated to further study the gene expression for those invading single tumor cells<sup>153, 154</sup>. This platform will be powerful to

illustrate the link between gene expression, molecular signaling, and phenotypes of single cancer cells and the altered biophysical microenvironment. Finally, to make an impact in our understanding on how biophysical cues in tumor cell invasion, a close collaboration among microsystems engineers and cancer biologists is critical for moving this field forward. This will require both parties to explore outside their field, attend meetings that they don't normally go to, and not be afraid to ask questions.

## Acknowledgments

This work is supported by grants from the National Center for Research Resources (5R21RR025801-03) and the NIH (8R21 GM103388-03, R21CA138366, R01CA221346, U54CA143876, and P01CA100324). We thank Hall for his drawing of the device in the Table of Contents entry.

## References

1. Chambers AF, Groom AC, MacDonald IC. *Nat Rev Cancer*. 2002; 2:563–572. [PubMed: 12154349]
2. Steeg PS. *Nat Med*. 2006; 12:895–904. [PubMed: 16892035]
3. Wirtz D, Konstantopoulos K, Searson PC. *Nat Rev Cancer*. 2011; 11:512–522. [PubMed: 21701513]
4. Paszek MJ, Weaver VM. *J Mammary Gland Biol Neoplasia*. 2004; 9:325–342. [PubMed: 15838603]
5. Paszek MJ, Zahir N, Johnson KR, Lakins JN, Rozenberg GI, Gefen A, Reinhart-King CA, Margulies SS, Dembo M, Boettiger D, Hammer DA, Weaver VM. *Cancer cell*. 2005; 8:241–254. [PubMed: 16169468]
6. Kumar S, Weaver VM. *Cancer and Metastasis Reviews*. 2009; 28:113–127. [PubMed: 19153673]
7. Joyce JA, Pollard JW. *Nat Rev Cancer*. 2009; 9:239–252. [PubMed: 19279573]
8. Bissell MJ, Hines WC. *Nat Med*. 2011; 17:320–329. [PubMed: 21383745]
9. Pickup MW, Mouw JK, Weaver VM. *EMBO reports*. 2014; 15:1243–1253. [PubMed: 25381661]
10. Marshall J. *Methods in molecular biology (Clifton, NJ)*. 2011; 769:97–110.
11. Hulkower KI, Herber RL. *Pharmaceutics*. 2011; 3:107–124. [PubMed: 24310428]
12. Albin A, Noonan DM. *Curr Opin Cell Biol*. 2010; 22:677–689. [PubMed: 20822888]
13. Roussos ET, Condeelis JS, Patsialou A. *Nat Rev Cancer*. 2011; 11:573–587. [PubMed: 21779009]
14. Zhou ZN, Boimel PJ, Segall JE. *Drug discovery today Disease models*. 2011; 8:95–112. [PubMed: 22081771]
15. Cekanova M, Rathore K. *Drug design, development and therapy*. 2014; 8:1911–1921.
16. Kim BJ, Wu M. *Annals of biomedical engineering*. 2012; 40:1316–1327. [PubMed: 22189490]
17. Polacheck WJ, Li R, Uzel SGM, Kamm RD. *Lab on a chip*. 2013; 13:2252–2267. [PubMed: 23649165]
18. Sung KE, Beebe DJ. *Advanced Drug Delivery Reviews*. 2014; 79–80:68–78.
19. Sackmann EK, Fulton AL, Beebe DJ. *Nature*. 2014; 507:181–189. [PubMed: 24622198]
20. Tien J. *Current Opinion in Chemical Engineering*. 2014; 3:36–41.
21. Boussommier-Calleja A, Li R, Chen MB, Wong SC, Kamm RD. *Trends Cancer*. 2016; 2:6–19. [PubMed: 26858990]
22. Hanahan D, Weinberg Robert A. *Cell*. 2011; 144:646–674. [PubMed: 21376230]
23. Friedl P, Alexander S. *Cell*. 2011; 147:992–1009. [PubMed: 22118458]
24. Meacham CE, Morrison SJ. *Nature*. 2013; 501:328–337. [PubMed: 24048065]
25. Wu J, Wu X, Lin F. *Lab on a Chip*. 2013; 13:2484–2499. [PubMed: 23712326]
26. Moraes C, Mehta G, Leshner-Perez SC, Takayama S. *Ann Biomed Eng*. 2012; 40:1211–1227. [PubMed: 22065201]
27. Young EW. *Integrative biology : quantitative biosciences from nano to macro*. 2013; 5:1096–1109. [PubMed: 23799587]

28. GABE IT, GAULT JH, ROSS J, MASON DT, MILLS CJ, SCHILLINGFORD JP, BRAUNWALD E. *Circulation*. 1969; 40:603–614. [PubMed: 5377202]
29. Popel AS, Johnson PC. *Annual review of fluid mechanics*. 2005; 37:43–69.
30. Hahn C, Schwartz MA. *Nature reviews Molecular cell biology*. 2009; 10:53–62. [PubMed: 19197332]
31. le Noble F, Moyon D, Pardanaud L, Yuan L, Djonov V, Matthijssen R, Breant C, Fleury V, Eichmann A. *Development (Cambridge, England)*. 2004; 131:361–375.
32. Culver JC, Dickinson ME. *Microcirculation (New York, NY)*. 1994; 17:164–178. 2010.
33. Lucitti JL, Jones EAV, Huang C, Chen J, Fraser SE, Dickinson ME. *Development (Cambridge, England)*. 2007; 134:3317–3326.
34. Davies PF. *Physiol Rev*. 1995; 75:519–560. [PubMed: 7624393]
35. Resnick N, Yahav H, Shay-Salit A, Shushy M, Schubert S, Zilberman LCM, Wofovitz E. *Progress in Biophysics and Molecular Biology*. 2003; 81:177–199. [PubMed: 12732261]
36. Li YSJ, Haga JH, Chien S. *Journal of Biomechanics*. 2005; 38:1949–1971. [PubMed: 16084198]
37. Chien S. *American journal of physiology Heart and circulatory physiology*. 2007; 292:H1209–1224. [PubMed: 17098825]
38. Dixon JB, Zawieja DC, Gashev AA, Coté GL. *BIOMEDO*. 2005; 10:064016–064016–064017.
39. Berk DA, Swartz MA, Leu AJ, Jain RK. *The American journal of physiology*. 1996; 270:H330–337. [PubMed: 8769769]
40. Jain RK. *Cancer research*. 1988; 48:2641–2658. [PubMed: 3282647]
41. Stylianopoulos T, Martin JD, Snuderl M, Mpekris F, Jain SR, Jain RK. *Cancer research*. 2013; 73:3833–3841. [PubMed: 23633490]
42. Jain RK, Martin JD, Stylianopoulos T. *Annual review of biomedical engineering*. 2014; 16:321–346.
43. Wiig H, Swartz MA. *Physiological Reviews*. 2012; 92:1005–1060. [PubMed: 22811424]
44. Wong SY, Hynes RO. *Cell cycle (Georgetown, Tex)*. 2006; 5:812–817.
45. Paduch R. *Cellular Oncology*. 2016; 39:397–410.
46. Chambers AF, Naumov GN, Varghese HJ, Nadkarni KV, MacDonald IC, Groom AC. *Surgical oncology clinics of North America*. 2001; 10:243–255. vii. [PubMed: 11382585]
47. Koumoutsakos P, Pivkin I, Milde F. *Annual Review of Fluid Mechanics*. 2013; 45:325–355.
48. Swartz MA, Skobe M. *Microscopy research and technique*. 2001; 55:92–99. [PubMed: 11596154]
49. Jain RK. *Cancer research*. 1987; 47:3039–3051. [PubMed: 3555767]
50. Chary SR, Jain RK. *Proceedings of the National Academy of Sciences of the United States of America*. 1989; 86:5385–5389. [PubMed: 2748592]
51. Ng CP, Helm CL, Swartz MA. *Microvascular research*. 2004; 68:258–264. [PubMed: 15501245]
52. Helm CLE, Fleury ME, Zisch AH, Boschetti F, Swartz MA. *Proceedings of the National Academy of Sciences of the United States of America*. 2005; 102:15779–15784. [PubMed: 16249343]
53. Helm CL, Zisch A, Swartz MA. *Biotechnology and bioengineering*. 2007; 96:167–176. [PubMed: 17133613]
54. Butler TP, Grantham FH, Gullino PM. *Cancer research*. 1975; 35:3084–3088. [PubMed: 1182701]
55. Hompland T, Ellingsen C, Øvrebø KM, Rofstad EK. *Cancer research*. 2012; 72:4899–4908. [PubMed: 23027087]
56. Jain RK, Baxter LT. *Cancer research*. 1988; 48:7022–7032. [PubMed: 3191477]
57. Boucher Y, Baxter LT, Jain RK. *Cancer research*. 1990; 50:4478–4484. [PubMed: 2369726]
58. Jain RK. *Science*. 1996; 271:1079–1080. [PubMed: 8599082]
59. Heldin CH, Rubin K, Pietras K, Ostman A. *Nat Rev Cancer*. 2004; 4:806–813. [PubMed: 15510161]
60. Lunt SJ, Fyles A, Hill RP, Milosevic M. *Future Oncology*. 2008; 4:793–802. [PubMed: 19086846]
61. Shields JD, Fleury ME, Yong C, Tomei AA, Randolph GJ, Swartz MA. *Cancer cell*. 2007; 11:526–538. [PubMed: 17560334]
62. Adrian CS, Melody AS. *Physical Biology*. 2011; 8:015012. [PubMed: 21301060]

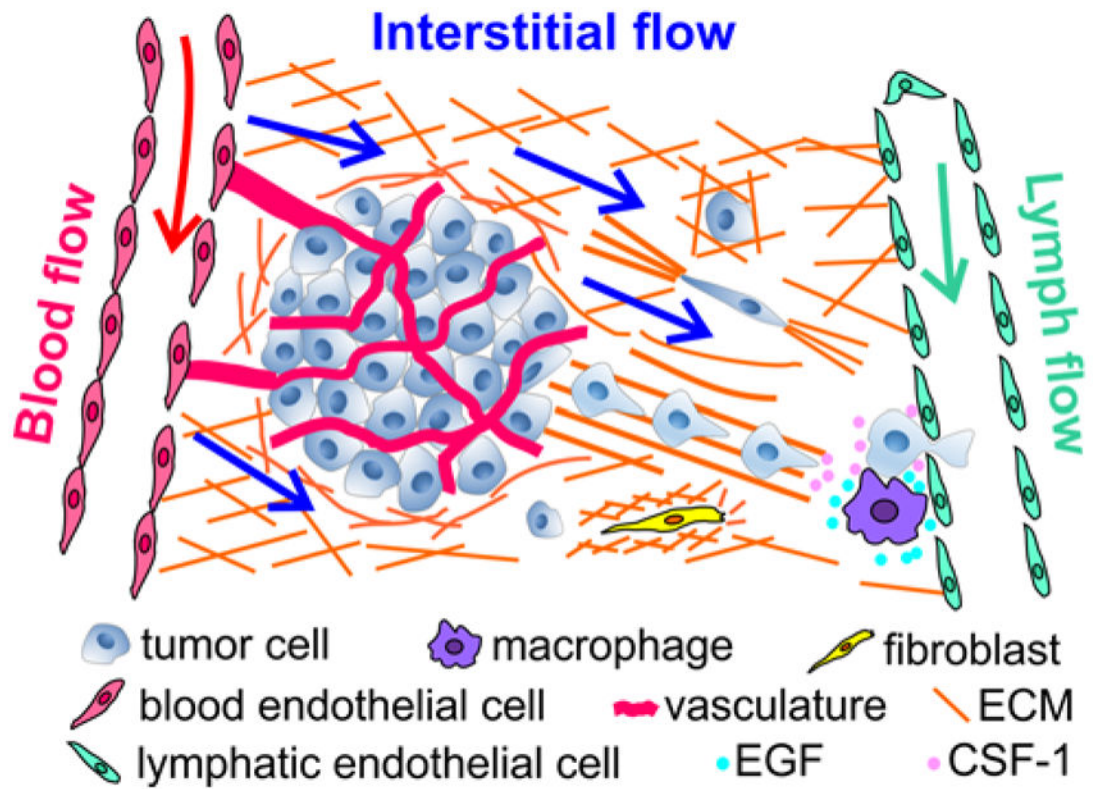
63. Munson JM, Bellamkonda RV, Swartz MA. *Cancer research*. 2013; 73:1536–1546. [PubMed: 23271726]
64. Kingsmore KM, Logsdon DK, Floyd DH, Peirce SM, Purow BW, Munson JM. *Integrative biology : quantitative biosciences from nano to macro*. 2016; doi: 10.1039/c6ib00167j
65. Polacheck WJ, German AE, Mammoto A, Ingber DE, Kamm RD. *Proceedings of the National Academy of Sciences*. 2014; 111:2447–2452.
66. Shieh AC, Rozansky HA, Hinz B, Swartz MA. *Cancer research*. 2011; 71:790–800. [PubMed: 21245098]
67. Lu P, Weaver VM, Werb Z. *The Journal of Cell Biology*. 2012; 196:395–406. [PubMed: 22351925]
68. Pathak A, Kumar S. *Integrative biology : quantitative biosciences from nano to macro*. 2011; 3:267–278. [PubMed: 21210057]
69. Chang JM, Moon WK, Cho N, Yi A, Koo HR, Han W, Noh DY, Moon HG, Kim SJ. *Breast Cancer Research and Treatment*. 2011; 129:89–97. [PubMed: 21681447]
70. Boyd NF, Lockwood GA, Byng JW, Trichler DL, Yaffe MJ. *Cancer Epidemiol Biomarkers Prev*. 1998; 7:1133–1144. [PubMed: 9865433]
71. Acerbi I, Cassereau L, Dean I, Shi Q, Au A, Park C, Chen YY, Liphardt J, Hwang ES, Weaver VM. *Integrative biology : quantitative biosciences from nano to macro*. 2015; 7:1120–1134. [PubMed: 25959051]
72. Kirschmann DA, Seftor EA, Fong SF, Nieva DR, Sullivan CM, Edwards EM, Sommer P, Csiszar K, Hendrix MJ. *Cancer research*. 2002; 62:4478–4483. [PubMed: 12154058]
73. Levental KR, Yu H, Kass L, Lakins JN, Egeblad M, Erler JT, Fong SFT, Csiszar K, Giaccia A, Weninger W, Yamauchi M, Gasser DL, Weaver VM. *Cell*. 2009; 139:891–906. [PubMed: 19931152]
74. Condeelis J, Segall JE. *Nat Rev Cancer*. 2003; 3:921–930. [PubMed: 14737122]
75. Weigelin B, Bakker GJ, Friedl P. *Intravital*. 2012; 1:32–43. [PubMed: 29607252]
76. Alexander S, Weigelin B, Winkler F, Friedl P. *Current Opinion in Cell Biology*. 2013; 25:659–671. [PubMed: 23896198]
77. Gehler S, Baldassarre M, Lad Y, Leight JL, Wozniak MA, Riching KM, Eliceiri KW, Weaver VM, Calderwood DA, Keely PJ. *Molecular Biology of the Cell*. 2009; 20:3224–3238. [PubMed: 19458194]
78. Hall MS, Alisafaei F, Ban E, Feng X, Hui C-Y, Shenoy VB, Wu M. *Proceedings of the National Academy of Sciences*. 2016; doi: 10.1073/pnas.1613058113
79. Provenzano PP, Eliceiri KW, Campbell JM, Inman DR, White JG, Keely PJ. *BMC Medicine*. 2006; 4:38. [PubMed: 17190588]
80. Conklin MW, Eickhoff JC, Riching KM, Pehlke CA, Eliceiri KW, Provenzano PP, Friedl A, Keely PJ. *Am J Pathol*. 2011; 178:1221–1232. [PubMed: 21356373]
81. Gaggioli C, Hooper S, Hidalgo-Carcedo C, Grosse R, Marshall JF, Harrington K, Sahai E. *Nat Cell Biol*. 2007; 9:1392–1400. [PubMed: 18037882]
82. Gritsenko PG, Ilina O, Friedl P. *The Journal of pathology*. 2012; 226:185–199. [PubMed: 22006671]
83. Wolf K, Alexander S, Schacht V, Coussens LM, von Andrian UH, van Rheenen J, Deryugina E, Friedl P. *Seminars in Cell & Developmental Biology*. 2009; 20:931–941. [PubMed: 19682592]
84. Doyle AD, Wang FW, Matsumoto K, Yamada KM. *J Cell Biol*. 2009; 184:481–490. [PubMed: 19221195]
85. Friedl P, Sahai E, Weiss S, Yamada KM. *Nature reviews Molecular cell biology*. 2012; 13:743–747. [PubMed: 23072889]
86. Chang, Stephanie S., Guo, W-h, Kim, Y., Wang, Y-l. *Biophysical Journal*. 2013; 104:313–321. [PubMed: 23442853]
87. Chrobak KM, Potter DR, Tien J. *Microvascular research*. 2006; 71:185–196. [PubMed: 16600313]
88. Nguyen DHT, Stapleton SC, Yang MT, Cha SS, Choi CK, Galie PA, Chen CS. *Proceedings of the National Academy of Sciences*. 2013; 110:6712–6717.
89. Wong AD, Searson PC. *Cancer research*. 2014; 74:4937–4945. [PubMed: 24970480]



90. Jimenez-Torres JA, Beebe DJ, Sung KE. *Methods in molecular biology* (Clifton, NJ). 2016; 1458:59–69.
91. Zheng Y, Chen J, Craven M, Choi NW, Totorica S, Diaz-Santana A, Kermani P, Hempstead B, Fischbach-Teschl C, López JA, Stroock AD. *Proceedings of the National Academy of Sciences*. 2012; 109:9342–9347.
92. Buchanan CF, Verbridge SS, Vlachos PP, Rylander MN. *Cell Adhesion & Migration*. 2014; 8:517–524. [PubMed: 25482628]
93. Bischel LL, Lee SH, Beebe DJ. *Journal of laboratory automation*. 2012; 17:96–103. [PubMed: 22357560]
94. Bischel LL, Young EWK, Mader BR, Beebe DJ. *Biomaterials*. 2013; 34:1471–1477. [PubMed: 23191982]
95. Bischel LL, Sung KE, Jiménez-Torres JA, Mader B, Keely PJ, Beebe DJ. *The FASEB Journal*. 2014; 28:4583–4590. [PubMed: 25077562]
96. Golden AP, Tien J. *Lab Chip*. 2007; 7:720–725. [PubMed: 17538713]
97. Bellan LM, Singh SP, Henderson PW, Porri TJ, Craighead HG, Spector JA. *Soft Matter*. 2009; 5:1354–1357.
98. Miller JS, Stevens KR, Yang MT, Baker BM, Nguyen D-HT, Cohen DM, Toro E, Chen AA, Galie PA, Yu X, Chaturvedi R, Bhatia SN, Chen CS. *Nat Mater*. 2012; 11:768–774. [PubMed: 22751181]
99. Kolesky DB, Truby RL, Gladman AS, Busbee TA, Homan KA, Lewis JA. *Advanced Materials*. 2014; 26:3124–3130. [PubMed: 24550124]
100. Bertassoni LE, Cecconi M, Manoharan V, Nikkhah M, Hjortnaes J, Cristino AL, Barabaschi G, Demarchi D, Dokmeci MR, Yang Y, Khademhosseini A. *Lab on a Chip*. 2014; 14:2202–2211. [PubMed: 24860845]
101. Sobrino A, Phan DTT, Datta R, Wang X, Hachey SJ, Romero-López M, Gratton E, Lee AP, George SC, Hughes CCW. *Scientific Reports*. 2016; 6:31589. [PubMed: 27549930]
102. Moya ML, Hsu Y-H, Lee AP, Hughes CCW, George SC. *Tissue Engineering Part C: Methods*. 2013; 19:730–737. [PubMed: 23320912]
103. Phan DTT, Wang X, Craver BM, Sobrino A, Zhao D, Chen JC, Lee LYN, George SC, Lee AP, Hughes CCW. *Lab on a Chip*. 2017; 17:511–520. [PubMed: 28092382]
104. Kim S, Chung M, Jeon NL. *Biomaterials*. 2016; 78:115–128. [PubMed: 26691234]
105. Gerlowski LE, Jain RK. *Microvascular research*. 1986; 31:288–305. [PubMed: 2423854]
106. Price GM, Wong KHK, Truslow JG, Leung AD, Acharya C, Tien J. *Biomaterials*. 2010; 31:6182–6189. [PubMed: 20537705]
107. Jeon JS, Bersini S, Gilardi M, Dubini G, Charest JL, Moretti M, Kamm RD. *Proceedings of the National Academy of Sciences*. 2015; 112:214–219.
108. Song JW, Munn LL. *Proceedings of the National Academy of Sciences*. 2011; 108:15342–15347.
109. Zhang Q, Liu T, Qin J. *Lab on a Chip*. 2012; 12:2837–2842. [PubMed: 22648473]
110. Zervantonakis IK, Hughes-Alford SK, Charest JL, Condeelis JS, Gertler FB, Kamm RD. *Proceedings of the National Academy of Sciences*. 2012; 109:13515–13520.
111. Ehsan SM, Welch-Reardon KM, Waterman ML, Hughes CC, George SC. *Integrative biology : quantitative biosciences from nano to macro*. 2014; 6:603–610. [PubMed: 24763498]
112. Pisano M, Triacca V, Barbee KA, Swartz MA. *Integrative Biology*. 2015; 7:525–533. [PubMed: 25896438]
113. Roeder BA, Kokini K, Sturgis JE, Robinson JP, Voytik-Harbin SL. *J Biomech Eng*. 2002; 124:214–222. [PubMed: 12002131]
114. Storm C, Pastore JJ, MacKintosh FC, Lubensky TC, Janmey PA. *Nature*. 2005; 435:191–194. [PubMed: 15889088]
115. Polacheck WJ, Charest JL, Kamm RD. *Proceedings of the National Academy of Sciences*. 2011; 108:11115–11120.
116. Haessler U, Teo JC, Foretay D, Renaud P, Swartz MA. *Integrative biology : quantitative biosciences from nano to macro*. 2012; 4:401–409. [PubMed: 22143066]

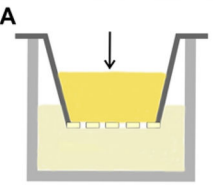
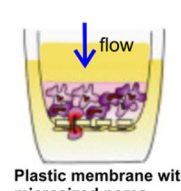
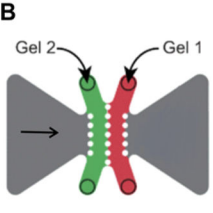
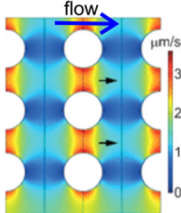
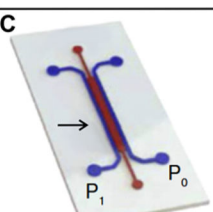
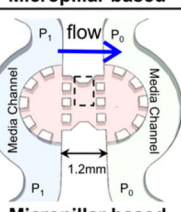
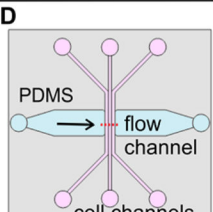
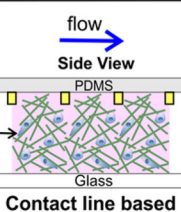
117. Tung CK, Krupa O, Apaydin E, Liou JJ, Diaz-Santana A, Kim BJ, Wu M. *Lab Chip*. 2013; 13:3876–3885. [PubMed: 23917952]
118. Huang YL, Tung C-k, Zheng A, Kim BJ, Wu M. *Integrative Biology*. 2015; 7:1402–1411. [PubMed: 26235230]
119. Raub CB, Unruh J, Suresh V, Krasieva T, Lindmo T, Gratton E, Tromberg BJ, George SC. *Biophysical Journal*. 2008; 94:2361–2373. [PubMed: 18065452]
120. Yang YL, Motte S, Kaufman LJ. *Biomaterials*. 2010; 31:5678–5688. [PubMed: 20430434]
121. Piotrowski-Daspit AS, Tien J, Nelson CM. *Integrative Biology*. 2016; 8:319–331. [PubMed: 26853861]
122. Friedl P, Wolf K. *Nat Rev Cancer*. 2003; 3:362–374. [PubMed: 12724734]
123. Friedl P, Locker J, Sahai E, Segall JE. *Nat Cell Biol*. 2012; 14:777–783. [PubMed: 22854810]
124. Patsialou A, Bravo-Cordero JJ, Wang Y, Entenberg D, Liu H, Clarke M, Condeelis JS. *Intravital*. 2013; 2:e25294. [PubMed: 25013744]
125. Rizvi I, Gurkan UA, Tasoglu S, Alagic N, Celli JP, Mensah LB, Mai Z, Demirci U, Hasan T. *Proceedings of the National Academy of Sciences of the United States of America*. 2013; 110:E1974–E1983. [PubMed: 23645635]
126. Nelson MT, Short A, Cole SL, Gross AC, Winter J, Eubank TD, Lannutti JJ. *BMC Cancer*. 2014; 14:825. [PubMed: 25385001]
127. Milano, Daniel F., Ngai, Nicholas A., Muthuswamy, Senthil K., Asthagiri, Anand R. *Biophysical Journal*. 2016; 110:1886–1895. [PubMed: 27119647]
128. Lee P, Lin R, Moon J, Lee LP. *Biomedical microdevices*. 2006; 8:35–41. [PubMed: 16491329]
129. Riching KM, Cox BL, Salick MR, Pehlke C, Riching AS, Ponik SM, Bass BR, Crone WC, Jiang Y, Weaver AM, Eliceiri KW, Keely PJ. *Biophys J*. 2014; 107:2546–2558. [PubMed: 25468334]
130. Sung KE, Su G, Pehlke C, Trier SM, Eliceiri KW, Keely PJ, Friedl A, Beebe DJ. *Biomaterials*. 2009; 30:4833–4841. [PubMed: 19540580]
131. Lanfer B, Freudenberg U, Zimmermann R, Stamov D, Korber V, Werner C. *Biomaterials*. 2008; 29:3888–3895. [PubMed: 18606448]
132. Han W, Chen S, Yuan W, Fan Q, Tian J, Wang X, Chen L, Zhang X, Wei W, Liu R, Qu J, Jiao Y, Austin RH, Liu L. *Proceedings of the National Academy of Sciences*. 2016; 113:11208–11213.
133. Vader D, Kabla A, Weitz D, Mahadevan L. *PloS one*. 2009; 4:e5902. [PubMed: 19529768]
134. Kim J, Staunton JR, Tanner K. *Advanced materials (Deerfield Beach, Fla)*. 2016; 28:132–137.
135. Ilina O, Bakker GJ, Vasaturo A, Hofmann RM, Friedl P. *Phys Biol*. 2011; 8:015010. [PubMed: 21301056]
136. Kraning-Rush CM, Carey SP, Lampi MC, Reinhart-King CA. *Integrative biology : quantitative biosciences from nano to macro*. 2013; 5:606–616. [PubMed: 23388698]
137. Wolf K, te Lindert M, Krause M, Alexander S, te Riet J, Willis AL, Hoffman RM, Figdor CG, Weiss SJ, Friedl P. *The Journal of Cell Biology*. 2013; 201:1069–1084. [PubMed: 23798731]
138. Isermann P, Davidson PM, Sliz JD, Lammerding J. *Current protocols in cell biology / editorial board, Juan S Bonifacino ... [et al]*. 2012; CHAPTER(Unit22.16-Unit22.16)
139. Davidson PM, Sliz J, Isermann P, Denais C, Lammerding J. *Integrative Biology*. 2015; 7:1534–1546. [PubMed: 26549481]
140. Denais CM, Gilbert RM, Isermann P, McGregor AL, te Lindert M, Weigelin B, Davidson PM, Friedl P, Wolf K, Lammerding J. *Science*. 2016; doi: 10.1126/science.aad7297
141. Skau CT, Fischer RS, Gurel P, Thiam HR, Tubbs A, Baird MA, Davidson MW, Piel M, Alushin GM, Nussenzweig A, Steeg PS, Waterman CM. *Cell*. 2016; 167:1571–1585.e1518. [PubMed: 27839864]
142. Miron-Mendoza M, Seemann J, Grinnell F. *Biomaterials*. 2010; 31:6425–6435. [PubMed: 20537378]
143. Cross VL, Zheng Y, Won Choi N, Verbridge SS, Sutermaster BA, Bonassar LJ, Fischbach C, Stroock AD. *Biomaterials*. 2010; 31:8596–8607. [PubMed: 20727585]
144. Raub CB, Suresh V, Krasieva T, Lyubovitsky J, Mih JD, Putnam AJ, Tromberg BJ, George SC. *Biophys J*. 2007; 92:2212–2222. [PubMed: 17172303]

145. Roy R, Boskey A, Bonassar LJ. *Journal of biomedical materials research Part A*. 2010; 93:843–851. [PubMed: 19658163]
146. Mason BN, Starchenko A, Williams RM, Bonassar LJ, Reinhart-King CA. *Acta biomaterialia*. 2013; 9:4635–4644. [PubMed: 22902816]
147. Cassereau L, Miroshnikova YA, Ou G, Lakins J, Weaver VM. *Journal of Biotechnology*. 2015; 193:66–69. [PubMed: 25435379]
148. Kim BJ, Hannanta-anan P, Chau M, Kim YS, Swartz MA, Wu M. *PloS one*. 2013; 8:e68422. [PubMed: 23869217]
149. Bhattacharjee N, Urrios A, Kang S, Folch A. *Lab on a Chip*. 2016; 16:1720–1742. [PubMed: 27101171]
150. Gjorevski N, Nelson CM. *Biophys J*. 2012; 103:152–162. [PubMed: 22828342]
151. Legant WR, Miller JS, Blakely BL, Cohen DM, Genin GM, Chen CS. *Nature methods*. 2010; 7:969–971. [PubMed: 21076420]
152. Irianto J, Xia Y, Pfeifer CR, Athirasala A, Ji J, Alvey C, Tewari M, Bennett RR, Harding SM, Liu AJ, Greenberg RA, Discher DE. *Current Biology*. 2017; 27:210–223. [PubMed: 27989676]
153. Shembekar N, Chaipan C, Utharala R, Merten CA. *Lab on a Chip*. 2016; 16:1314–1331. [PubMed: 27025767]
154. Ahrberg CD, Manz A, Chung BG. *Lab on a Chip*. 2016; 16:3866–3884. [PubMed: 27713993]
155. Fischer M, Franzeck UK, Herrig I, Costanzo U, Wen S, Schiesser M, Hoffmann U, Bollinger A. *American Journal of Physiology - Heart and Circulatory Physiology*. 1996; 270:H358–H363.
156. Yuan F, Salehi HA, Boucher Y, Vasthare US, Tuma RF, Jain RK. *Cancer research*. 1994; 54:4564–4568. [PubMed: 8062241]
157. Kamoun WS, Chae S-S, Lacorre DA, Tyrell JA, Mitre M, Gillissen MA, Fukumura D, Jain RK, Munn LL. *Nature methods*. 2010; 7:655–660. [PubMed: 20581828]
158. Leunig M, Yuan F, Menger MD, Boucher Y, Goetz AE, Messmer K, Jain RK. *Cancer research*. 1992; 52:6553–6560. [PubMed: 1384965]
159. Dafni H, Israely T, Bhujwalla ZM, Benjamin LE, Neeman M. *Cancer research*. 2002; 62:6731–6739. [PubMed: 12438274]
160. Fu BM, Shen S. *Microvascular research*. 2004; 68:51–62. [PubMed: 15219420]
161. Yuan W, Lv Y, Zeng M, Fu BM. *Microvascular research*. 2009; 77:166–173. [PubMed: 18838082]
162. Scallan JP, Huxley VH. *J Physiol*. 2010; 588:243–254. [PubMed: 19917564]
163. Yuan F, Leunig M, Berk DA, Jain RK. *Microvascular research*. 1993; 45:269–289. [PubMed: 8321142]
164. Dreher MR, Liu W, Michelich CR, Dewhirst MW, Yuan F, Chilkoti A. *J Natl Cancer Inst*. 2006; 98:335–344. [PubMed: 16507830]
165. Albelda SM, Sampson PM, Haselton FR, McNiff JM, Mueller SN, Williams SK, Fishman AP, Levine EM. *Journal of Applied Physiology*. 1988; 64:308–322. [PubMed: 2451657]
166. Swartz MA, Fleury ME. *Annu Rev Biomed Eng*. 2007; 9:229–256. [PubMed: 17459001]
167. Levick JR. *Quarterly journal of experimental physiology (Cambridge, England)*. 1987; 72:409–437.
168. Ramanujan S, Pluen A, McKee TD, Brown EB, Boucher Y, Jain RK. *Biophysical Journal*. 2002; 83:1650–1660. [PubMed: 12202388]
169. Michel CC, Curry FE. *Physiol Rev*. 1999; 79:703–761. [PubMed: 10390517]



**Figure 1.**

Important biophysical parameters in the tumor microenvironment (TME): intramural (blood and lymph) flows, interstitial flow, and the architectural support of extracellular matrices (ECM). Important biochemical parameters: cytokine gradients, nutrients, and oxygen, and multiple other cell types (stromal, immune, and endothelial cells).

	Device design	Key feature	Advantages/ Disadvantages	Biological insights
Modified Boyden Chamber		 Plastic membrane with micro-sized pores	+ Easy to use + High throughput  - Average and population level results	Interstitial flow induced breast tumor cells invasion via autologous chemotaxis [61].
Microfluidic Platform		 Micropillar based	+ Tunable flow rates + Capable to recreate a more complex tumor environment + Allow single cell dynamic studies  - Nonuniform fluid flow through the ECM	Only a subpopulation of breast tumor cells respond to interstitial flow because of the heterogeneous nature of cancer cells [116].
		 Micropillar based	+ Capable to recreate a more complex tumor environment + Allow single cell dynamic studies  - Nonuniform fluid flow through the ECM	Interstitial flow induced directional migration of breast tumor cells via chemosensory receptors and mechanosensing molecules [65, 115].
		 Contact line based	+ Uniform flow through the ECM + Can incorporate both interstitial and intramural flows + Allow single cell dynamic studies  - Restrict to surface properties	Interstitial flow promoted amoeboid over mesenchymal motilities of breast tumor cells via adhesion molecules [118].

**Figure 2.** Modeling interstitial flows in tumor cell invasion studies. A, Modified Boyden chamber platform. Tumor cell embedded biomatrix is introduced into a Boyden Chamber insert, which is placed in a well. The gravitational pressure, provided by the fluid level difference between the fluid within the insert and that in the surrounding well, drives the interstitial flow. The invasion rate is marked by the number of cells transmigrated through the porous membrane at the bottom of the insert. B,C,D: Three different microfluidic platforms for modeling interstitial flows. B. In this device, lines of pillars with circular cross section of diameter  $500\ \mu\text{m}$  are used to confine collagen. Interstitial flow is driven by gravity along the horizontal direction. Numerically simulated flow field is shown in the right panel of B. C: In this device, lines of square pillars, each with a cross section of  $250\ \mu\text{m} \times 250\ \mu\text{m}$ , are used to confine collagen. Gravity driven flow is introduced horizontally across collagen matrices. D: In this device, contact lines with cross section of  $10\ \mu\text{m} \times 5\ \mu\text{m}$  are used to confine collagen within the cell channel. Interstitial flow is introduced using a syringe pump in the horizontal flow channel. Image on the right side of panel A is reproduced from reference <sup>61</sup>, with permission from Elsevier. Images in B are reproduced from reference <sup>116</sup> with permission from the Royal Society of Chemistry. Images in C are reproduced from references <sup>65, 115</sup>

with permission from the Proceedings of the National Academy of Sciences, and images in D are reproduced from reference <sup>118</sup> with permission from the Royal Society of Chemistry.

Author Manuscript

Author Manuscript

Author Manuscript

Author Manuscript



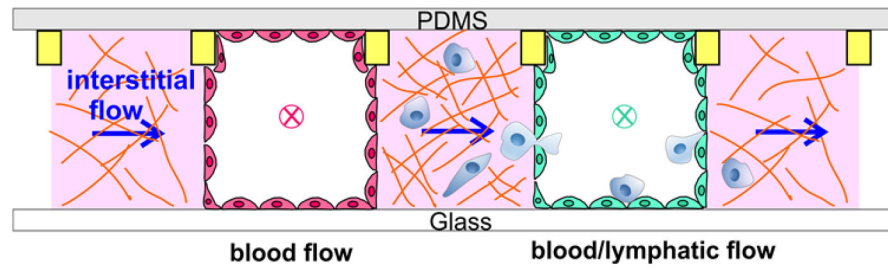


**Figure 3.**

Illustration of a microfluidic model recreating the biophysical microenvironment for tumor cell invasion studies. ECM or tumor cell embedded ECM (pink) is introduced into three wall-less channels confined by contact lines (yellow rectangular, not to scaled). Blood vessel (red) and lymphatic vessel (green) are formed by growing a layer of blood and lymphatic EC cells respectively. Blood and lymph flows are introduced into two vascular vessels (direction marked by x), and interstitial flow is introduced horizontally (direction marked by an arrow).

**Table 1**

Intramural and interstitial flow rates and vessel diameters measured in healthy tissue using animal models, and in tumors using both animal and human models.

	Healthy tissue	Tumor
<b>Intramural flow</b>	<p><u>Arterioles:</u><sup>29</sup> diameter 15–60<math>\mu</math>m: 7–12 mm/s</p> <p><u>Capillaries:</u><sup>29</sup> diameter 5<math>\mu</math>m: 0.2 mm/s</p> <p><u>Venules:</u><sup>29</sup> diameter 18–72<math>\mu</math>m: 0.2–2.4 mm/s</p> <p><u>Microlymphatic vessels:</u><sup>38</sup> diameter 100 <math>\mu</math>m: 1–7 mm/s</p> <p><u>Lymphatic capillaries:</u><sup>39, 155</sup> diameter 55 <math>\mu</math>m: 0–29 <math>\mu</math>m/s</p>	<p><u>Blood vessels in mammary carcinoma:</u><sup>156</sup> diameter 7–63<math>\mu</math>m: 0–0.8 mm/s</p> <p><u>Blood vessels in glioma:</u> diameter 8–55<math>\mu</math>m: 0–0.5 mm/s<sup>156</sup> diameter 1–100<math>\mu</math>m: 0.001–10 mm/s<sup>157</sup></p> <p><u>Blood vessels in adenocarcinoma:</u><sup>158</sup> arterioles 9–10<math>\mu</math>m: 0.59–0.7 mm/s capillaries 6–8<math>\mu</math>m: 0.09–0.27 mm/s venules 10–26<math>\mu</math>m: 0.09–0.22 mm/s</p>
<b>Interstitial flow</b>	<p><u>Rabbit ear tissue:</u><sup>50</sup> 0.59<math>\pm</math>0.16 <math>\mu</math>m/s</p>	<p><u>VX2 carcinoma:</u> 0.55 <math>\pm</math> 0.16 <math>\mu</math>m/s<sup>50</sup></p> <p><u>C6-pTET-VEGF tumor:</u> 0.1–0.5 <math>\mu</math>m/s<sup>159</sup></p> <p><u>Cervical carcinoma:</u> 1–7 <math>\mu</math>m/s<sup>55</sup></p> <p><u>Melanoma:</u> 1–9 <math>\mu</math>m/s</p> <p><u>Nonmetastatic squamous carcinoma:</u> 5–25 <math>\mu</math>m/s</p> <p><u>Metastatic squamous carcinoma:</u> 10–55 <math>\mu</math>m/s</p>

**Table 2**

Vascular permeability and hydraulic conductivity of ECM measured *in vivo* and *in vitro*. Vascular permeability (or permeability coefficient across an endothelium layer),  $P$ , is the ratio of solute flux and solute concentration gradient across the endothelium layer <sup>169</sup>. Hydraulic conductivity,  $K'$  is the ratio of fluid flux and pressure gradient as defined in Darcy's law. Specific hydraulic conductivity ( $K$ ) is  $K' \eta$ , where  $\eta$  is the fluid viscosity.

	In vivo		In vitro modeling
	Healthy tissue	Tumor	
<b>Permeability across blood and lymphatic endothelium [cm/s]</b>	<p>Capillaries and postcapillary venules <sup>105</sup>: (for dextran MW=150,000) <math>7.26 \pm 3.29 \times 10^{-8}</math></p> <p>Postcapillary venules <sup>160</sup>: (for sodium fluorescein) <math>1.4 \pm 0.11 \times 10^{-5}</math> (for <math>\alpha</math>-Lactalbumin) <math>4.4 \pm 0.5 \times 10^{-7}</math> (for BSA) <math>4.9 \pm 0.32 \times 10^{-8}</math></p> <p>Postcapillary venules <sup>161</sup>: (for 4kDa dextran) <math>9.2 \pm 4.6 \times 10^{-7}</math> (for 10kDa dextran) <math>3.1 \pm 1.3 \times 10^{-7}</math> (for 20kDa dextran) <math>2.4 \pm 1.0 \times 10^{-7}</math> (for 40kDa dextran) <math>1.9 \pm 1.1 \times 10^{-7}</math> (for 70kDa dextran) <math>1.5 \pm 0.5 \times 10^{-7}</math></p> <p>Venules <sup>162</sup>: (for RSA) <math>3.5 \pm 1.0 \times 10^{-7}</math></p> <p>Collecting lymphatic vessels <sup>162</sup>: (for RSA) <math>4.0 \pm 1.0 \times 10^{-7}</math></p>	<p>Capillaries and postcapillary venules in VX2 carcinoma <sup>105</sup>: (for dextran MW=150,000) <math>5.7 \pm 3.9 \times 10^{-7}</math></p> <p>Microvascular in adenocarcinoma <sup>163</sup>: (for BSA) <math>6.06 \pm 4.30 \times 10^{-7}</math></p> <p>Arterioles and venules in mammary adenocarcinoma <sup>156</sup>: (for BSA) <math>1.7 \pm 0.6 \times 10^{-7}</math> <math>2.9 \pm 1.5 \times 10^{-7}</math> <math>1.9 \pm 0.5 \times 10^{-7}</math></p> <p>Arterioles and venules in glioblastoma <sup>156</sup>: (for BSA) <math>3.8 \pm 1.2 \times 10^{-7}</math> <math>1.1 \pm 0.5 \times 10^{-8}</math></p> <p>Vasculature in squamous carcinoma <sup>164</sup>: (for 3.3kDa dextran) <math>1.54 \times 10^{-5}</math> (for 40kDa dextran) <math>9.5 \times 10^{-7}</math> (for 2MDa dextran) <math>1.7 \times 10^{-7}</math> (for BSA) <math>4.9 \times 10^{-7}</math></p>	<p><b>In transwell:</b> EC monolayer <sup>165</sup>: (for Albumin) <math>5.6 \times 10^{-6}</math></p> <p><b>In microfluidics:</b> Hollow EC lumen with tumor cells <sup>110</sup>: (for 10kDa) <math>4.08 \pm 1.11 \times 10^{-5}</math> (for 70kDa) <math>7.5 \pm 0.93 \times 10^{-6}</math></p> <p>Single blood EC tube <sup>87, 91</sup> (for BSA) <math>5.5 \pm 3.5 \times 10^{-6}</math> <math>7.9 \pm 3.5 \times 10^{-6}</math> (for 70kDa dextran) <math>4.1 \pm 0.5 \times 10^{-6}</math> (for 332Da fluorescein) <math>7.0 \pm 1.5 \times 10^{-6}</math></p> <p>Self-assembled blood vessels <sup>101, 107</sup>: (for 70kDa dextran) <math>8.9 \pm 3.1 \times 10^{-7}</math> (for 70kDa dextran) <math>4.5 \times 10^{-7}</math> (for 150kDa dextran) <math>1.2 \times 10^{-7}</math></p>
<b>Hydraulic conductivity of ECM</b>	<b>Hydraulic conductivity (<math>K'</math>) [<math>cm^2/mmHg \cdot s</math>]</b> (From references <sup>166</sup> and <sup>167</sup> )		<b>Specific hydraulic conductivity (<math>K</math>) [<math>cm^2</math>]</b>
	<p>Abdominal muscle: <math>1.5 \times 10^{-7}</math> to <math>7.8 \times 10^{-7}</math></p> <p>Dermis: <math>5.3 \times 10^{-8}</math></p> <p>Tail skin: <math>7 \times 10^{-7}</math> to <math>1.5 \times 10^{-6}</math></p>	<p>HSTS 26T sarcoma: <math>9 \times 10^{-8}</math></p> <p>U87 glioblastoma: <math>6.5 \times 10^{-7}</math></p> <p>LS174T carcinoma: <math>4.5 \times 10^{-7}</math></p> <p>MCalV carcinoma: <math>2.5 \times 10^{-6}</math></p>	<p>Type I collagen matrices <sup>143</sup>: 3mg/mL: <math>3 \times 10^{-7}</math> 8mg/mL: <math>3.5 \times 10^{-8}</math> 10mg/mL: <math>7.5 \times 10^{-9}</math> 15mg/mL: <math>9 \times 10^{-10}</math> 20mg/mL: <math>1.5 \times 10^{-10}</math></p> <p>Type I collagen matrices <sup>168</sup>: 10mg/mL: <math>1 \times 10^{-11}</math></p>